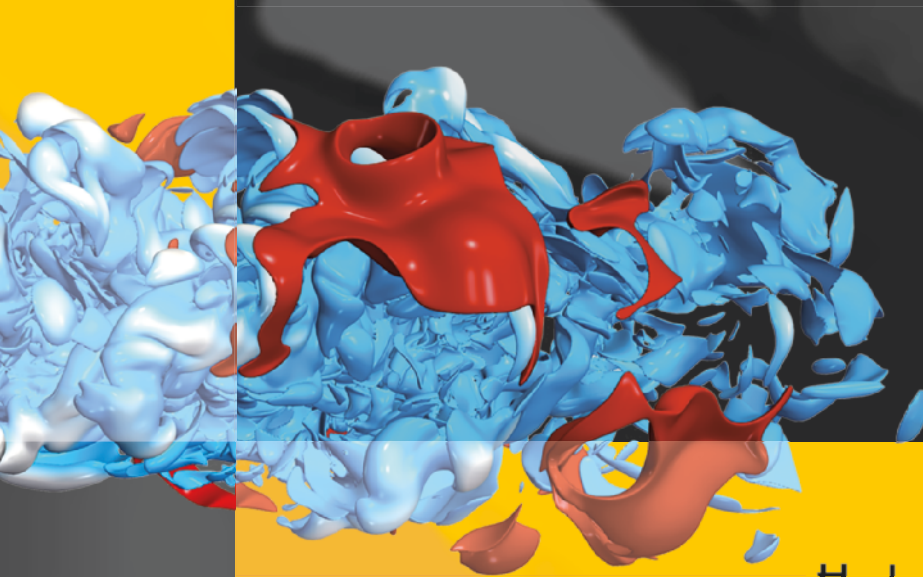Wolfgang E. Nagel
Dietmar H. Kröner
Michael M. Resch *Editors*

High Performance Computing
in Science and Engineering '19

H L R **I** S

Springer

High Performance Computing in Science
and Engineering '19

Wolfgang E. Nagel · Dietmar H. Kröner · Michael M. Resch

Editors

High Performance Computing in Science and Engineering '19

Transactions of the High Performance Computing Center, Stuttgart (HLRS) 2019

Editors
Wolfgang E. Nagel
Zentrum für Informationsdienste und
Hochleistungsrechnen (ZIH)
Technische Universität Dresden
Dresden, Germany

Dietmar H. Kröner
Abteilung für Angewandte Mathematik
Universität Freiburg
Freiburg, Germany

Michael M. Resch
Höchstleistungsrechenzentrum Stuttgart
(HLRS)
Universität Stuttgart
Stuttgart, Germany

Contents

Molecules, Interfaces, and Solids

Materials Science

Reactive Flows

Computational Fluid Dynamics

Physics

Prof. Dr. Peter Nielaba

In this section, seven physics projects are presented, which achieved important scientific results in 2018/19 by using Hazel Hen at the HLRS and ForHLR II of the Steinbuch Center.[1]

Fascinating new results are being presented in the following pages on astrophysical systems (simulations of galaxy formation, analysis of the first image of a black hole and binary merger evolutions, and of photoionization and atomic, molecular and optical collision processes), soft matter systems (interaction between proteins and hydrophilic polymers), many body quantum systems (simulations of ultracold quantum systems), and high energy physics systems (hadronic contributions to the muon magnetic moment).

The studies of the astrophysical systems have focused on galaxy formation, analysis of the first image of a black hole and binary merger evolutions, and on photoionization and atomic, molecular, and optical collision processes.

A. Pillepich, D. Nelson, V. Springel, R. Pakmor, L. Hernquist, M. Vogelsberger, R. Weinberger, S. Genel, F. Marinacci, P. Torrey, J. Naiman from Heidelberg (A.P.), Garching (D.N., V.S., R.P.), Cambridge USA (L.H., R.W., J.N., M.V.), New York (S.G.), Bologna (F.M.), and Gainesville (P.T.) present in their project *GCS-DWAR* recent results from the TNG50 run, the third and final volume of the cosmological, magnetohydrodynamical simulations in the IllustrisTNG project (AREPO code), with over 20 billion resolution elements and a spatial resolution of 100 parsecs. The authors report on the results of the recently completed TNG50 simulations, reaching the red shift $z = 0$, the present day. TNG50 is bridging the gap between large cosmological volumes and better resolved zoom galaxies. Results include the abundances of dwarf galaxies in the first few billion years of the history of the Universe and the kinematic properties of the Hα and molecular gas within and around galaxies at intermediate redshift, as well as predictions for our improved understanding of galaxy evolution. The results will be made publicly available to the astronomy community.

R. Gold and L. Rezzolla from the University of Frankfurt contributed in their project *BBHDISKS* to the analysis of the first image of a black hole by the Event

---

Horizon Telescope (EHT) collaboration and developed a code further for the study of two black holes in orbit around each other. In their studies, they use a black hole accretion code (BHAC) for solving the general relativistic magntohydrodynamic (GRMHD) equations, which is based on the MPI-AMRVAC toolkit, using a fully adaptive block-based (oct-) tree mesh refinement with a fixed refinement factor of two between successive levels, and which is interfaced with many analysis tools and external codes. The project topics include the general behavior of magnetized, turbulent gas moving around or falling onto a black hole system, the observational appearance of such systems, the predictions for systems with two black holes in magnetized gas, and the advancement of computational tools to tackle such systems in the contexts of both ideal and resistive magnetohydrodynamics on non-homogenous and dynamical grids. A GRMHD image library has been build for the analysis of the EHT results, and the computation of initial data for the space–time metric was an important step for the planned investigations of accreting binary black holes.

B. M. McLaughlin, C. P. Ballance, R. T. Smyth, M. S. Pindzola, P. C. Stancil, J. F. Babb and A. Müller from the Universities of Belfast (B.M.M., C.P.B., R.T.S.), Auburn (M.S.P.), Georgia (P.C.S.), Cambridge USA (J.F.B.), and Giessen (A.M.) investigated in their project *GCS-PMP2* atomic, molecular, and optical collisions on petaflop machines, relevant for astrophysical applications, for magnetically confined fusion and plasma modeling, and as theoretical support for experiments and satellite observations. The Schrödinger and Dirac equations have been solved with the R-matrix or R-matrix with pseudo-states approach, and the time-dependent close-coupling method has been used for the studies of ion-atom excitations and electron-impact ionizations. Various systems and phenomena have been investigated in detail such as the photoionization of Rb^+ and Rb^2+ ions, the electron impact excitation of Fe II, the proton impact on sodium atoms, the $CS-H^2$ diatomic collision, and the dicarbon formation by radiative association.

Studies of the soft matter systems have focused on the interaction of proteins with hydrophilic polymers.

T. Schäfer, C. Muhl, M. Barz, F. Schmid and G. Settanni from the University of Mainz investigated in their project *Flexadfg* the thermodynamics and kinetics of the interactions between proteins and hydrophilic polymers by Molecular Dynamics simulations, using the program NAMD and CHARMM force fields with CMAP correction, a cell-list algorithm, and a smooth particle mesh Ewald (PME) method, and a modified TIP3P model for water molecules. In particular, the adsorption of poly-(ethylene-glycol) (PEG), poly-sarcosine (PSar), and poly-alanine (PAla) on the surface of proteins was studied in order to determine their usefulness as coating agents for nanoparticles. The authors find that the pattern of interactions with the surface amino acids does not change much for the different polymers, and that the amount of adsorbed polymers and the residence time on the protein surface varies significantly, depending on the conformational properties.

In the last granting period, quantum mechanical properties of high energy physics systems have been investigated as well as the quantum many body dynamics of trapped bosonic systems.

A. U. J. Lode, O. E. Alon, L. S. Cederbaum, B. Chakrabarti, B. Chatterjee, R. Chitra, A. Gammal, S. K. Haldar, M. L. Lekala, C. Leveque, R. Lin, P. Molignini, L. Papariello, and M. C. Tsatsos from the Universities of Wien (A.U.J.L, C.L.), Haifa (O.E.A., S.K.H.), Heidelberg (L.S.C.), Kolkata (B.C.), Kanpur (B.C.), Zürich (R.C., R.L., P.M., L.P.), Sao Paulo (A.G., M.C.T.), Pretoria (M.L.L.) studied in their project *MCTDHB* trapped ultracold atomic systems by their method termed multiconfigurational time-dependent Hartree for bosons (MCTDHB and MCTDH-X software packages). The principal investigators investigated the fermionization and crystallization of ultracold strongly interacting bosons, correlations of bosons with strong dipolar interactions, cavity-induced phase transitions of ultracold bosons in high-finesse cavities, the dimensionality of the variance of Bose Einstein condensates (BECs) in annular confinements, the dynamics of BECs with long-ranged interactions in a bosonic Josephson junction, the dynamics of BECs in an asymmetric bosonic Josephson junction, and the variance of BECs in anharmonic traps.

Two projects (GCS-HQCD and GCS-MUMA) investigated hadronic contributions to the muon magnetic moment with very interesting results. The principal investigators and project contributors of the project GCS-HQCD were M. Ce, A. Gerardin, G. von Hippel, B. Horz, H. B. Meyer, D. Mohler, K. Ottnad, S. Schaefer, J. Wilhelm, and H. Wittig from the Universitiy of Mainz (M.C., A.G., G.v.H.,B.H., H.B.M., D.M., K.O., J.W., H.W.), from DESY (A.G., S.S.) and from the Lawrence Berkeley National Laboratory (B.H.), the principal investigators and project contributors of project GCS-MUMA were K. Szabo, Cs. Torok, K. Miura, L. Parato, and L. Varnhorst. Since only the project GCS-HQCD was participating in the 22nd Results and Review Workshop of the HLRS (2019), only the report of this project can be presented in the present volume. The interest in the anomalous magnetic moment of the muon is motivated by the consequences for a theory beyond the standard model. In project GCS-HQCD, leading systematic uncertainties in standard model predictions from hadronic contributions are computed by Lattice Quantum Chromodynamics simulations, using the Hybrid Monte Carlo (HMC) algorithm in the openQCD code. Calculations of the hadronic vacuum polarization contribution to the anomalous magnetic moment based on Coordinated Lattice Simulations consortium gauge ensembles with 2+1 dynamical flavors with improved Wilson quarks have been done and reveal an effect on the anomalous magnetic moment in the order of about $7 \cdot 10^{-8}$.

The TNG50 Simulation: Highly-Resolved Galaxies in a Large Cosmological Volume to the Present Day

Annalisa Pillepich, Dylan Nelson, Volker Springel, Rüdiger Pakmor, Lars Hernquist, Mark Vogelsberger, Rainer Weinberger, Shy Genel, Federico Marinacci, Paul Torrey, and Jill Naiman

---

A. Pillepich (✉)
Max-Planck-Institut für Astronomie, Königstuhl 17, 69117 Heidelberg, Germany
e-mail: pillepich@mpia-hd.mpg.de; pillepich@mpia.de

D. Nelson · V. Springel · R. Pakmor
Max-Planck-Institut für Astrophysik, Karl-Schwarzschild-Str. 1, 85741 Garching, Germany
e-mail: dnelson@mpa-garching.mpg.de

V. Springel
e-mail: vspringel@mpa-garching.mpg.de

R. Pakmor
e-mail: rpakmor@mpa-garching.mpg.de

L. Hernquist · R. Weinberger · J. Naiman
Harvard-Smithsonian Center for Astrophysics, 60 Garden Street, Cambridge, MA 02138, USA
e-mail: lars@cfa.harvard.edu

R. Weinberger
e-mail: rainer.weinberger@cfa.harvard.edu

J. Naiman
e-mail: jill.naiman@cfa.harvard.edu

M. Vogelsberger
MIT Kavli Institute for Astrophysics and Space Research, Department of Physics,
Massachusetts Institute of Technology, Cambridge, MA 02139, USA
e-mail: mvogelsb@mit.edu

S. Genel
Center for Computational Astrophysics, Flatiron, 162 Fifth Avenue, New York, NY 10010, USA
e-mail: shygenelastro@gmail.com

F. Marinacci
Department of Physics and Astronomy, University of Bologna, via Gobetti 93/2,
40129 Bologna, Italy
e-mail: federico.marinacci2@unibo.it

P. Torrey
Department of Physics, University of Florida, 2001 Museum Rd., Gainesville, FL 32611, USA
e-mail: paul.torrey@ufl.edu

Abstract Large-volume cosmological hydrodynamical simulations of galaxy formation enable us to theoretically follow the co-evolution of thousands of galaxies while directly outputting the observable signatures that result from the complex and highly non-linear process of cosmic structure formation. Here we present the first results from the TNG50 run, an unprecedented 'next generation' cosmological, magnetohydrodynamical simulation that we have recently brought to completion on the Hazel Hen supercomputer. TNG50 is the third and final volume of the IllustrisTNG project. With over 20 billion resolution elements it resolves spatial scales down to ~ 100 parsecs, following the co-evolution of dark matter, gas, stars, supermassive black holes and magnetic fields across the history of the Universe.

1 Introduction

The evolution and physical properties of galaxies depend on a rich set of physical ingredients: the laws of gravity; the nature of dark matter; the details of the growth of cosmological structures on the largest spatial scales; the interaction between radiation and cosmic gas and hence gas cooling and heating; the chemical and thermodynamical properties of the gas which forms stars and feeds the growth of super massive black holes; the evolution and death of stellar populations; and the non-linear effects and coupling of energy, momentum, and radiative feedback from stars and black holes. The diversity and complexity of the relevant physical processes can be followed in full generality only through cosmological hydrodynamical computer simulations. However, the enormous range of spatial and time scales, as well as the complexity of the physical processes involved, makes this a remarkable computational challenge. Significant progress has been made in this direction, as embodied in large-volume hydrodynamical projects such as Illustris [1–4], EAGLE [5, 6], and Horizon-AGN [7]. These have begun to generate plausible and diverse galaxy populations by combining ab-initio calculations with sub grid prescriptions of small-scale phenomena: run at 'kilo-parsec' spatial resolutions, these numerical experiments have reproduced a number of fundamental scaling relations and properties of observed galaxy populations. This zeroth order agreement has buttressed many theoretical investigations and predictions. At the same time, however, it has revealed many shortcomings in the current generation of models.

    IllustrisTNG is a 'next generation' series of large, cosmological, gravo-magneto-hydrodynamical simulations incorporating a comprehensive model for galaxy formation physics [8, 9]. It has been conducted over the past three years on the Hazel Hen machine at the High Performance Computing Center Stuttgart (HLRS) and supported by two Gauss Centre for Supercomputing allocations (GCS-ILLU in 2014, and GCS-DWAR in 2016). IllustrisTNG includes three flagship runs: TNG50, TNG100, and TNG300. The latter two have been completed within the first allocation and presented last year [10–14]. TNG50 is the most computational demanding of the three simulations by far: with a total of about 135M core hours, TNG50 has been recently

completed, reaching $z = 0$ (the current epoch, or present day) in April 2019. Here we showcase the first results from this project.

2   IllustrisTNG: Physical and Numerical Developments

The IllustrisTNG simulation project[1] extends the original Illustris simulation in two key ways. First, it alleviates most of the previous model deficiencies [15], i.e. tensions with respect to available observational data. Second, it expands upon the scope in all directions by executing simulations with higher resolution, of larger volumes, and with new physics.

2.1   Galaxy Formation in TNG: The Numerical Code

The IllustrisTNG simulation suite uses the AREPO code [16], which solves for the coupled evolution of self-gravity and magnetohydrodynamics [MHD; [17, 18]]. The former is computed with the spatially split Tree-PM approach, while the latter is based on a finite-volume method whose spatial discretization is a dynamic, unstructured, Voronoi tessellation. The scheme is quasi-Lagrangian (ALE) and second order in both space and time. It achieves high dynamic range through an individual particle time-stepping approach. In contrast to past cosmological simulations, IllustrisTNG now fundamentally includes a treatment of magnetic fields under the assumptions of ideal MHD [17, 18].

The AREPO code has been architected to execute large parallel astrophysical simulations. For instance, the TNG50 simulation reviewed here has been run on 16320 cores. At this scale the highly coupled, high dynamic range of the galaxy formation problem is particularly challenging: TNG50 captures a spatial dynamic range of $\sim 10^7$, while the time hierarchy necessitates evolution on timescales which differ by $\sim 10^4$. For numerical optimization reasons, over the past several years and in preparation for the TNG simulations, (i) the previous MUSCL-Hancock time integration scheme has been replaced with an approach following Heun's method [19], (ii) the method for obtaining gradients of primitive fluid quantities has been replaced with an iterative least-squares method, (iii) the long-range gravity FFT calculation now uses a new, column-based MPI-parallel FFT which improves scaling at high core numbers, and (iv) the gravity solver incorporates a new, recursive splitting of the N-body Hamiltonian into short- and long- timescale particle systems.

---

[1] http://www.tng-project.org.

2.2   Galaxy Formation in TNG: Physical Model

Cosmological hydrodynamical simulations such as TNG acknowledge that physics below a given spatial scale, of order a hundred to a few hundred parsecs, cannot be resolved and must be treated by approximate, sub-resolution models. This includes, most importantly, the process of star formation, the detailed action of individual supernova events, the formation and growth of supermassive blackholes, and the near-field coupling of blackhole feedback energy to the surroundings. Together, these components make up the updated TNG model for galaxy formation, which is described in [9] and [8]. We employ it unchanged (and invariant with numerical resolution) in all TNG simulations, including TNG50.

The physical framework includes models of the most important physical processes for the formation and evolution of galaxies; (i) gas radiative microphysics, including primordial (H/He) and metal-line cooling and heating with an evolving ultraviolet/x-ray background field, (ii) star formation in dense interstellar medium (ISM) gas, (iii) the evolution of stellar populations and chemical enrichment, tracking supernovae Ia, II, and AGB stars, and individual species: H, He, C, N, O, Ne, Mg, Si, and Fe, (iv) galactic-scale outflows launched by stellar feedback, (v) the formation, binary mergers, and gas accretion by supermassive blackholes, (vi) blackhole feedback, operating in a thermal mode at high accretion rates and a kinetic 'wind' mode at low accretion rates. Aspects (iv) and (vi) have been substantially revised in TNG, and we described the key changes in our previous report [20]. In short, galactic-scale outflows generated by stellar feedback are modeled using a kinetic wind approach [21] based on the energy available from Type II (core-collapse) supernovae. In TNG the directionality, thermal content, energy budget scaling with metallicity, and minimum launch velocity were all redesigned in order to better reflect available data constraints [full details in [8]]. Additionally, supermassive black holes (SMBHs) form in massive halos and subsequently inject large amounts of energy, as allowed by their instantaneous mass accretion rates as derived from their immediate neighborhoods. In TNG we introduced a new low-state kinetic wind feedback model, in the form of a time-pulsed, oriented, high-velocity 'wind', suggested to be a possibly crucial mechanism by recent theoretical as well as observational work [full details in [9]].

2.3   Early Results from TNG, Model Confirmations, and Predictions

Over the past year and a half, the TNG model has been shown to produce results that are consistent with a wide range of observational constraints, including regimes beyond those adopted for the model development. With respect to galactic structural and stellar population properties these include: the shape of the red sequence and blue cloud of SDSS galaxies [12]; the spatial clustering of active and passive galaxies

at the 1-halo and 2-halo term scales [11]; galaxy stellar mass functions up to $z \sim 4$ [10]; stellar sizes out to $z \sim 2$ split by star-forming vs. quiescent populations [22]; the scatter of Europium abundance in metal-poor stars in Milky Way-like systems [23]; the quenched galaxy population at both low [24] and high [25] redshift; the gas-phase mass-metallicity relation [26]; the dark matter fractions within massive galaxies at $z = 0$ in comparison to SLUGGS results [27]; and the visible light morphologies of galaxies versus Pan-STARRS data [28].

The IllustrisTNG model also produces a range of less common galaxies, i.e. it samples tails of the galaxy population. These include low surface brightness (LSB) galaxies [29] and ram-pressure stripped 'jellyfish' systems [30]. With respect to massive galaxy cluster, intra-cluster and circumgalactic medium properties we find broad agreement in: the relationship between total radio power and X-ray luminosity, total mass, and Sunyaev-Zel'dovich signal [13]; the distribution of metals versus radius in the intra-cluster medium [ICM; [31]]; the observed fraction of cool core vs. non-cool core clusters [32]; and the OVI content of the circumgalactic media around galaxies versus the COS-Halos and eCGM surveys [33].

IllustrisTNG is also returning novel insights on the formation and evolution of galaxies: for instance, on the universality of stellar mass profiles [10]; how star-forming and quenched galaxies take distinct evolutionary pathways across the galaxy size-mass plane [22]; that galaxies oscillate around the star formation main sequence and the mass-metallicity relations in an anti-correlated, time synchronized fashion [26]; that jellyfish galaxies are signaled by large-scale bow shocks in the surrounding intra-cluster medium [30]; how the metal enrichment of cluster galaxies is higher than field counterparts at fixed mass, even prior to infall [34]; the way in which baryonic processes modulate the matter power spectrum [11] and steepen the inner total density profiles of early-type galaxies [35]; and the properties of OVII, OVIII [33] and NeIX [36] absorption systems as detectable by future X-ray telescopes like ATHENA.

We have also generated mock 21-cm maps [37] and estimates of the molecular hydrogen (H2) abundance [38], also as a function of environment, in the local [39] and high-redshift Universe accessible with ALMA [40]. Finally, TNG provides a test bed to explore future observational applications of techniques such as machine learning: for example, using Deep Neural Networks to estimate galaxy cluster masses from Chandra X-ray mock images [41] or CNN-based optical morphological classification versus SDSS [42].

2.4   TNG50 Project Scope

TNG50 is the third and final volume of the IllustrisTNG project. This simulation occupies a unique combination of large volume and high resolution—its details and numerical properties are given in Table 1 in comparison to the TNG series as a whole, while Fig. 1 gives a visual comparison of the volumes. Our 50 Mpc box is sampled by 2160^3 dark matter particles (with masses of $4 \times 10^5 \, \mathrm{M_\odot}$) and 2160^3

Table 1 Details of the TNG50 simulation in comparison to its two larger volume counterparts

Run Name	Volume	N_{GAS}	N_{DM}	N_{TR}	m_{baryon}	m_{DM}	$\epsilon_{gas,min}$	$\epsilon_{DM,stars}$
	[Mpc^3]	–	–	–	[M$_\odot$]	[M$_\odot$]	[pc]	[pc]
TNG50	51.7^3	2160^3	2160^3	2160^3	8.5×10^4	4.5×10^5	74	**288**
TNG100	110.7^3	1820^3	1820^3	2×1820^3	1.4×10^6	7.5×10^6	185	740
TNG300	302.6^3	2500^3	2500^3	2500^3	1.1×10^7	5.9×10^7	370	1480
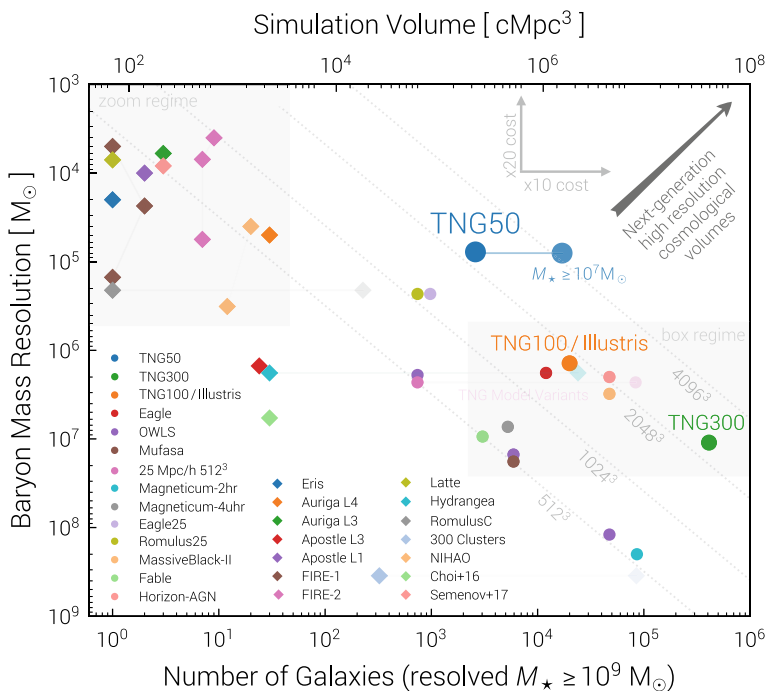
Fig. 1 The TNG50 simulation is a unique cosmological hydrodynamical simulation: it includes 2×2160^3 resolution elements, implying a baryonic mass resolution of $8.5 \times 10^4 M_\odot$ with adaptive gas softening down to 74 comoving parsecs. This approaches, or exceeds, the resolution of modern 'zoom' simulations of individual galaxies, while maintaining the statistical power and unbiased sampling of the full $\sim$50 cMpc cosmological volume. Here we show TNG50 (dark blue) in comparison to other cosmological volumes (circles) and zoom simulation suites (diamonds) at the current cosmological epoch (i.e. $z \sim 0$), based on the total number of resolved galaxies (a proxy for volume and statistics). Pushing towards the upper right corner represents the frontier of galaxy formation simulations, as well as extreme computational difficulty

initial gas cells (with masses of $8 \times 10^4 \, M_\odot$). The total number of resolution elements is therefore slightly over 20 billion. The *average* spatial resolution of star-forming interstellar medium (ISM) gas is $\sim$90 ($\sim$140) parsecs at $z = 1$ ($z = 6$). TNG50

has 2.5 times better spatial resolution, and 15 times better mass resolution, than TNG100 (or equivalently, original Illustris). This resolution approaches or exceeds that of modern 'zoom' simulations of individual galaxies [43, 44], while the volume contains $\sim 20{,}000$ resolved galaxies with $M_\star > 10^7\,\mathrm{M}_\odot$ (at $z = 1$).

At the time of writing, the TNG50 simulation has been evolved from the initial conditions of the Universe all the way to the current epoch, $z = 0$ (13.8 billion years after), and it is hence completed.

TNG50 contains roughly 200 Milky Way and Andromeda analogs, enabling detailed comparisons to our own galaxy at $z = 0$. It also hosts two massive galaxy clusters with a total mass $\sim 10^{14}\,\mathrm{M}_\odot$, i.e. Virgo-like analogs, and dozens of group sized halos at $\sim 10^{13}\,\mathrm{M}_\odot$. All of these massive objects are simulated at higher numerical resolution than in any previously published study, enabling studies not only of the gaseous halos and central galaxies, but also of the large populations of their satellite galaxies.

3 The TNG50 Simulation: Current Results and Outlook

The TNG50 simulation has been presented in the scientific literature with two introductory papers, focusing, respectively, on the internal structural and kinematical properties of star-forming galaxies across time [45] and on the gaseous outflows resulting from stellar and black hole feedback [46]. Another study based on the combination of TNG50 with the first two runs of the IllustrisTNG project (TNG100 and TNG300) has too been submitted for peer-review with the goal of quantifying the evolution of the stellar mass and luminosity functions of galaxies in anticipation of the observations with the James Webb Space Telescope (JWST) [47]. In the next Sections, we summarize selected highlights from these early TNG50 analyses and showcase ongoing and future investigations tailored at maximally exploit the TNG50 run and explored in a number of papers currently in preparation.

We can now analyze a fully representative, simulated galaxy population spanning $10^7 < M_\star/\mathrm{M}_\odot < 10^{11.5}$ across time, $0 < z < 10$. The high resolution of TNG50 is specifically exploited to investigate scales, regimes, and scientific questions not addressable using other cosmological simulations. This coverage in redshift range and galaxy stellar mass enables us to make quantitative predictions for signatures observable with JWST, now anticipated to launch in 2021, as well as recent ground-based IFU instruments such as MUSE and SINFONI, in addition to capturing the dynamics of gas, dark matter, and magnetic fields within and between galaxies. The key science drivers of TNG50 focus not only on the present day ($z = 0$), but also at earlier epochs, from cosmic noon ($z \sim 2$) through reionization ($z \sim 6$).

3.1 Uncovering Galactic Structure and Galaxy Kinematics

Studies of the stellar kinematics of star-forming galaxies are now common in the local
Universe e.g. with integral field spectroscopy (IFS) data from SAMI, MANGA, and
CALIFA. However, this is not yet viable at earlier cosmic epochs. The progenitors of
present-day galaxies are observed at $z \sim 1 - 2$ and characterized in their kinematics
from ground based telescopes using adaptive-optics techniques: these enable kilo-
parsec scale resolution but are based on tracing bright emission lines from hydrogen
(such as Hα) or metals (i.e. OIII). In other terms, such high-redshift observations
trace the kinematics of galactic gas instead of stars, as in [48]. In practice, at interme-
diate and early cosmic time (redshift $z > 0.3$), the observational analysis of galaxies
encounters a difficulty: galaxy morphologies are typically obtained through multi-
wavelength imaging surveys that trace the stellar light, while galaxy kinematics are
commonly obtained through Hα spectroscopy. Using TNG50, we are able to pro-
vide model predictions for projected radial profiles and resolved 2D maps of stellar
and gas density, star formation rate (Hα), stellar and gas line-of-sight velocity and
velocity dispersions [45]. We uncover outcomes of TNG50 for which the model has
not been in any way calibrated and is thus predictive. Furthermore, we can contrast
structural versus kinematical features, as well as the properties of the stellar versus
gaseous components of galaxies, by focusing on a redshift regime where such com-
parisons are currently prohibitive in observations, though soon to emerge, therefore
maximizing the predictive return of the TNG50 calculation.

In Fig. 2 we show the matter distribution and velocity fields of a randomly selected
galaxy at $z = 2$ from TNG50, one of thousands (see www.tng-project.org/explore/
gallery/ for a more comprehensive set of examples). From top to bottom, the panels
show the stellar component of the galaxy (in edge-on and face-on projections) and its
star-forming and gaseous component (also in edge-on and face-on projections). The
line-of-sight velocity of the galaxy in the edge-on projections (mid column, first and
third rows) is a proxy for the rotation of the galaxy and the corresponding rotation
curve is shown in the rightmost columns (first and third rows). The line-of-sight
velocity dispersion of the galaxy in the face-on projections (mid column, second and
bottom rows), on the other hand, represent the contribution of random (i.e. disordered,
non rotational, or even turbulent) local motions of stars and gas. Small scale structures
at sub-kiloparsec scales are easily resolved by TNG50, revealing rich morphological
and kinematical features. We can see, for example, how outflows generated from
the nuclear regions of disks leave signatures in the gas left behind, evidenced in the
central depressions because of the expulsion of gas through black hole feedabck. In
fact, despite their strong ordered rotation, galactic disks at intermediate redshifts $z \sim
1 - 3$ are highly turbulent gaseous reservoirs, characterized by velocity dispersion
fields that are remarkably less coherent in space than their stellar analogs (bottom
vs. second rows).

Galactic disks, however, settle with time. This is shown in Fig. 3 in terms of the
balance between ordered and disordered motions in TNG50 star-forming galaxies
as a function of redshifts. Orange curves and markers denote gas-based kinematics,
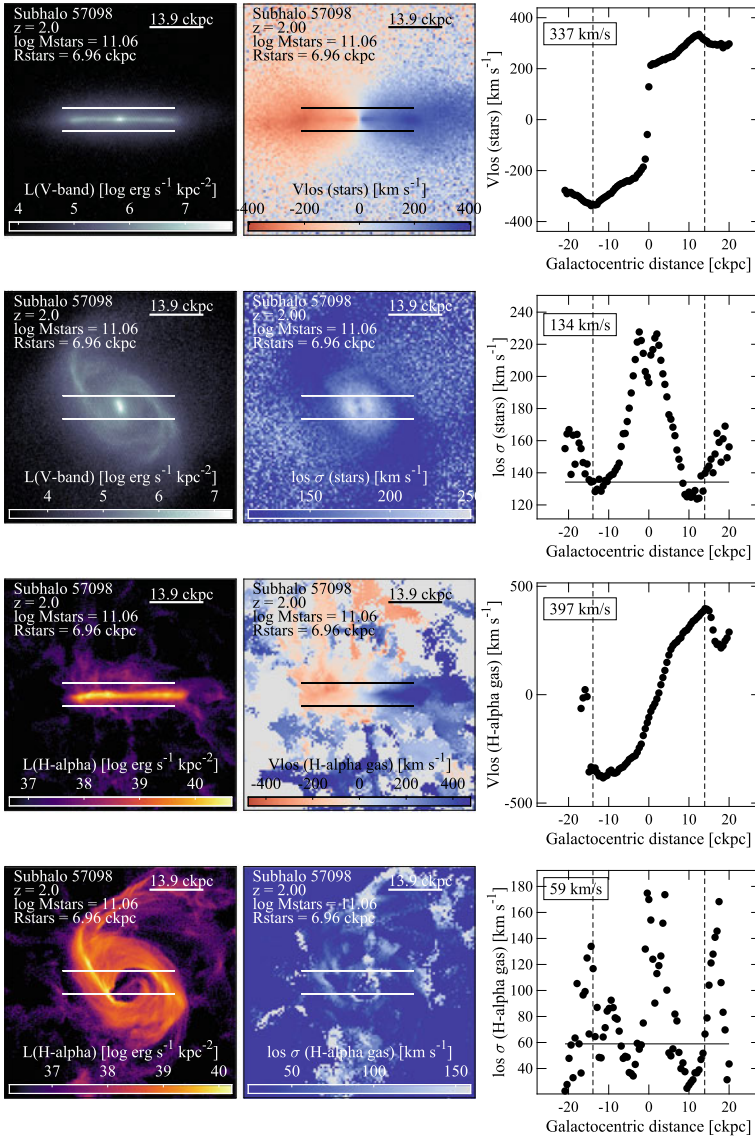
Fig. 2 One example of a massive galaxy at redshift 2 from the TNG50 simulation, randomly chosen among thousands [45]. The panels show V-band light maps, velocity maps and velocity profiles for the stellar component of the galaxy in edge-on (top row) and face-on (second row from the top) projections, together with the analog Hα light maps, velocity maps and velocity profiles for its star-forming and gaseous component (bottom two rwos). A more comprehensive set of examples is available on the IllustrisTNG website: www.tng-project.org/explore/gallery/
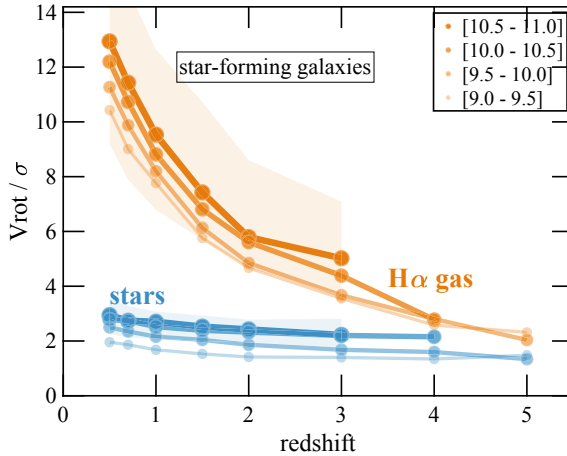
Fig. 3 Degree of ordered vs. turbulent motion (Vrot/σ) in TNG50 galaxies as a function of redshift in bins of galaxy stellar mass [45]. Solid curves and markers denote medians of the TNG50 Vrot/σ, for the Hα-emitting gas (orange) and the stellar component (blue), separately. Overall, the balance between ordered and disordered motions of the gaseous bodies increases substantially as the Universe evolves, and more so than the stellar counterparts

while blue curves indicate stellar-based kinematics, in bins of galaxy stellar mass. TNG50 star-forming galaxies host strongly rotating gaseous disks, more rotationally-supported the older the Universe: these trends are qualitatively consistent with current observations and constitute a non-trivial confirmation of the underlying physical model. Additionally, for the first time, this plot demonstrates that, at all times and masses, the dense gas component of star-forming galaxies is characterized by larger circular motions than the stellar material, with differences as large as a factor of several at low redshift and high mass. Such contrast, as a function of galaxy mass and cosmic time, can be directly tested against upcoming observational programs.

3.2 Gas-Dynamical Processes and Feedback-Driven Outflows

The kinematical and thermodynamical state of the gas within and around galaxies is a sensitive probe of galaxy formation physics, plasma physics, and even cosmology. Within very massive haloes, observations at X-ray and radio wavelengths reveal a rich level of detail and sub-substructure [49]. On galactic scales, energetic outflows driven out of galaxies reveal astrophysical feedback processes in action. These are associated with supernova explosions and to the activity of super massive blackholes residing at the center of galaxies—both are considered fundamental for the regulation of star formation in galaxies. The resolution of TNG50 enables a detailed study of
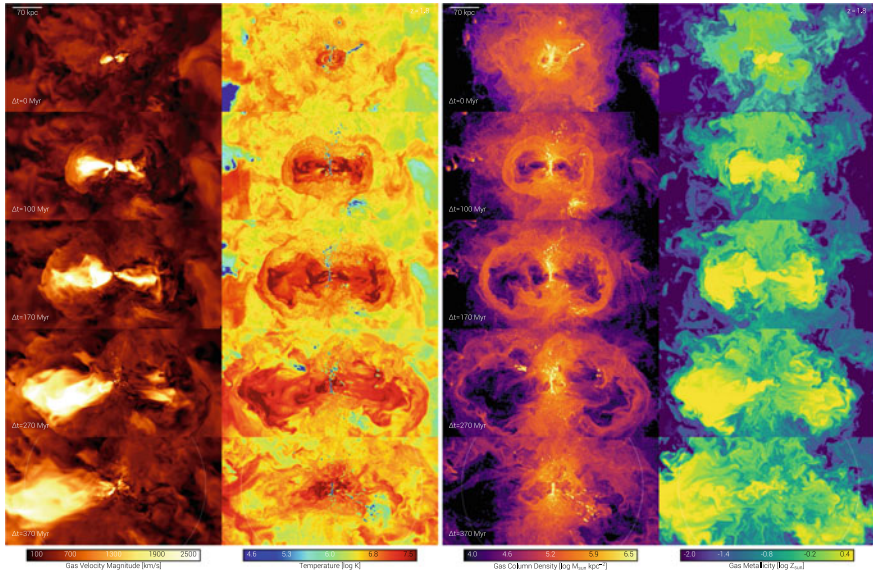
Fig. 4 We show a black hole feedback event driving a large-scale, galactic outflow in TNG50 [46]. From top to bottom shows the time evolution, with five snapshots ∼ 100 Myr apart, starting from $z \simeq 2$. Depicted is a single massive galaxy with a stellar mass of $10^{11.4}$ M$_\odot$, which is currently 'quenching' its star formation. From left to right: gas velocity, temperature, density, and metallicity, all on the halo scale (virial radius as white circles). The galaxy itself is oriented vertically, edge-on, and is visible as the small, cold disk at the center of each image. The central black hole has a mass of $10^{8.7}$ M$_\odot$ and is driving a large-scale collimated outflow in the kinetic 'wind' feedback mode

the properties of gas motions within and around galaxies across an unprecedented range of galaxy types, masses, environments, and cosmic epochs.

In [46] we use TNG50 to quantify the properties of galactic outflows in the cosmological setting and with respect to the galaxies from which they arise, by focusing on the way in which outflows shape the galaxy population as a whole, modulate galaxy evolution, and generate associated observational signatures. Figure 4 visualizes, for example, the time evolution of a strong outflow driven by a massive black hole in TNG50 originating from a massive galaxy at $z \sim 2$. Maps show gas velocity, gas temperature, gas density and gas metallicity (from left to right), with time progressing downwards, each row roughly 100 Myr apart. In our model, energy injection from the black hole produces a high-velocity, large-scale, and highly collimated (directional) outflow, which reaches speeds exceeding 2500 km/s even as it crosses the halo virial radius, qualitatively similar to some observed in the real Universe. By showing the highly resolved structure of an individual galaxy, we emphasize here that TNG50 allows us to connect small-scale (i.e. few hundred pc) feedback and large- scale (i.e. few hundred kpc) outflows.

Our TNG50 calculation predicts that gaseous outflow velocities increase with a galaxy's stellar mass and that outflows are faster at higher redshift. The phase struc-

ture of galactic winds is also complex, and we demonstrate that the TNG model can produce high velocity, multi-phase outflows which include cool, dense components. Importantly, we show how the relative simplicity of model inputs (and scalings) at the injection scale produces complex behavior at galactic and halo scales. For example, despite isotropic wind launching, outflows exhibit natural collimation and an emergent bipolarity [46].

3.3 Demographics of Galaxies in the First Few Billion Years

Galaxies form and evolve not in isolation but within the large-scale structure that emerges according to the theory of hierarchical assembly and collapse [50]. Energetic feedback processes (see Section above) result in radiation from their constituent stars and black holes, enabling galaxies to alter the ionization state of the surrounding gas, driving the cosmic Reionization of the intergalactic medium that is believed to have occurred within the first billion year of cosmic evolution. However, to quantitatively pin down the details of this final *phase transition* in the history of the Universe, we must first confront theoretical predictions with observations of the most basic quantity that defines the galaxy population: its abundance, i.e. the galaxy luminosity function, measuring the number density of galaxies as a function of their luminosities at different wavelengths and at different redshifts. This in turn can be used to quantify the escape fraction of ionizing radiation from galaxies that could have re-ionized the Universe.

The upcoming JWST promises to open a new window into the high redshift Universe to study faint and distant galaxies during the epoch of Reionization and later. Particularly, JWST will quantify the galaxy population and galaxy luminosity functions at higher redshifts than ever before: it will also decidedly increase the statistical sample sizes of high redshift galaxies. As TNG50 evolves all of the relevant baryonic and non-baryonic components self-consistently together and up to spatial scales of tens of mega-parsec scales, we can provide expectations for the high redshift galaxy population and Universe in general.

In [47], we exploit the large dynamic range of the whole IllustrisTNG simulation suite, TNG50, TNG100, and TNG300, to derive multi-band galaxy luminosity functions from $z = 1$ to $z = 10$. We put particular emphasis on the exploration of different dust attenuation models to determine galaxy luminosity functions for the rest-frame ultraviolet (UV), and apparent wide NIRCam bands. In Fig. 5, we visualize the outcome of our most detailed dust model, based on continuum Monte Carlo radiative transfer calculations employing observationally calibrated dust properties. The top row depicts light maps a random sample of TNG50 galaxies at $z \sim 1$, based on a combination of apparent F070W, F090W, F115W filter fluxes. The high numerical resolutions of TNG50 reveals sub-kpc details as well as lanes of dust that absorb light from the central bright regions. The bottom left panel shows the intrinsic and dust attenuated spectral energy distributions of two random TNG50 galaxies at $z = 2$, together with the filters of the NIRCam instrument on board JWTS. The bottom right
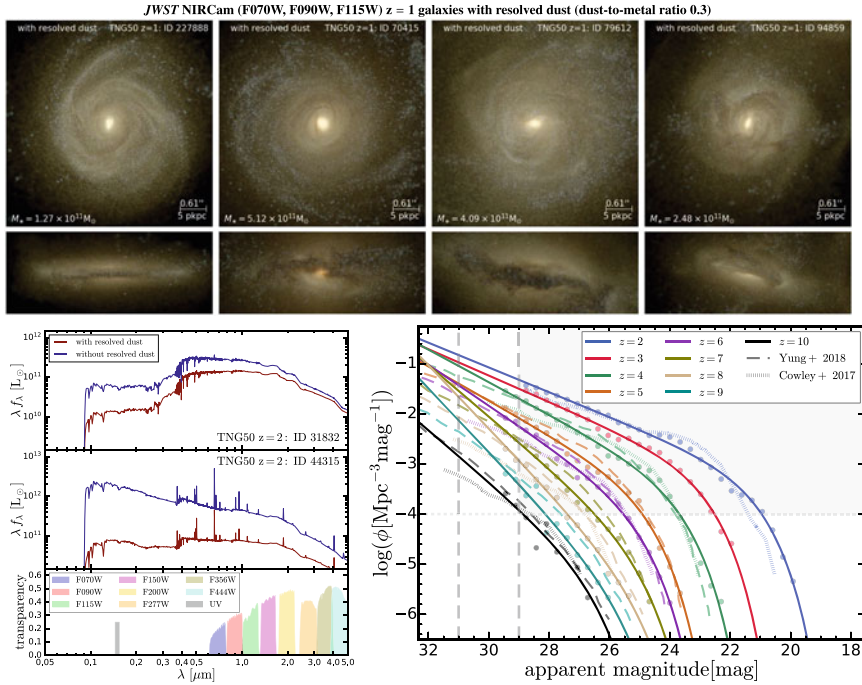
Fig. 5 Top: Face-on and edge-on images of a few randomly-chosen TNG50 galaxies at $z = 2$, as would be seen by JWST NIRCam [47]. These images include the effects of resolved dust attenuation calculated via a post-processing, Monte Carlo dust radiative transfer calculation employing 10^7 photon packets per wavelength on a wavelength grid spanning 0.05μm to 5μm. Dust radiative transfer effects are critical: in fact, the light from the central bright regions of the various galaxies is strongly absorbed and scattered due to dust. Bottom left: Spectral energy distribution for two example galaxies from TNG50 at $z = 2$, including the intrinsic spectral energy distribution (blue) and the dust attenuated spectrum (red). The bottom inset shows the relevant transmission functions of the different bands, including the ultraviolet and eight wide JWST NIRCam filters. Bottom right: Apparent luminosity functions at different redshifts predicted by the IllustrisTNG calculations, as will be observed in the JWST NIRCam F200W band. Markers show simulation data, and lines functional fits, including Schechter fits from currently-available observations for comparison

panel provides the F200W band luminosity functions and best-fit Schechter function parameters for the predicted NIRCam wide filter apparent luminosity functions as predicted by the IllustrisTNG model. For the F200W NIRCam band, we predict that JWST will detect about 80 (∼200) galaxies with a signal-to-noise ratio of 10 (5) within the NIRCam field of view for a total exposure time of 10^5s in the redshift range $z = 8 \pm 0.5$. These numbers will drop to about 10 (40) for a shorter exposure time, e.g. with 10^4s [47].

3.4   Further Ongoing TNG50 Explorations

The synthetic Universe of TNG50 encompasses thousands of realistic and well-resolved galaxies, spanning a variety of masses, environments, evolutionary and interaction stages, and fully described in terms of their gaseous, stellar, dark matter, and black hole content. The aforementioned scientific highlights represent a sample of the diverse applications that the TNG50 calculation enables. With a physical resolution which is unprecedented for such a cosmological volume, TNG50 bridges the gap towards 'zoom' simulations of individual galaxies and resolves systems as small as the 'dwarf' satellites of galaxies like our own Milky Way. Simultaneously, the large volume of the simulation box enables statistically significant and unbiased analyses of the galaxy population and of the large scale structure. With TNG50 brought to completion in April 2019 (i.e. to the current epoch, $z = 0$), we can now tackle all the originally identified fundamental science drivers of the TNG50 calculation: (1) The formation, evolution, and properties of dwarf galaxies; (2) Milky Way-like galaxies and their satellites systems; (3) Galaxy evolution in massive cluster environments and the intra-cluster medium; and (4) Low-density circumgalactic and intergalactic gas, from halo to cosmological scales (Fig. 6).

Numerous projects based on the TNG50 output are currently in progress, and extend in topic far beyond the originally identified science goals. These include the quantification of the turbulence in the diffuse gas of the universe and within the intra-halo medium of groups and clusters of galaxies; the amplification of magnetic fields

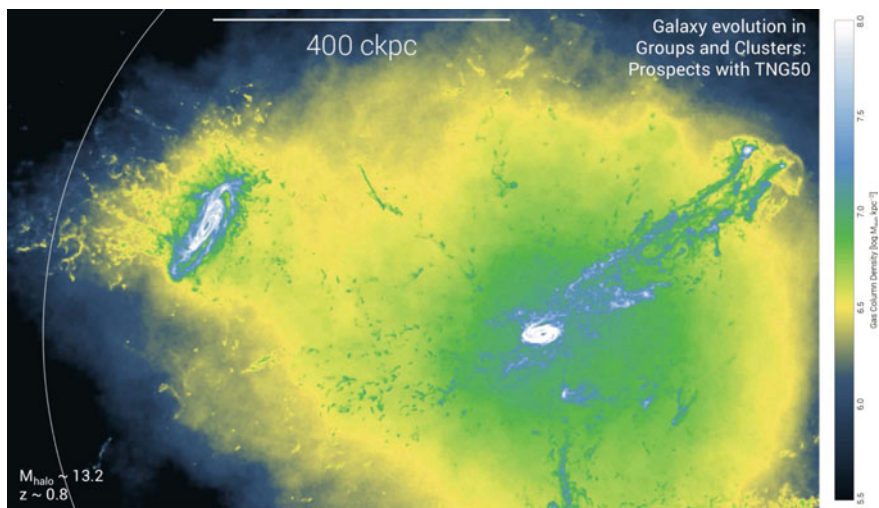**Fig. 6** The gas density in projection within a $10^{13.2}\,\mathrm{M_\odot}$ halo at $z \sim 0.8$ from the TNG50 cosmological volume. The virial radius of the halo extends to hundreds kilo parsecs distances from its central massive galaxy. Other galaxies are visibly undergoing 'stripping' of their gas reservoirs into long tails due to the interaction with the central object and the diffuse intra-cluster medium

in high-redshift galaxies and the magnetic field topology within galaxy clusters; the properties, emergence and comparison to observations of stellar haloes surrounding Milky Way-like galaxies; the onset of bars in disk-like galaxies; the X-ray scaling relations of the gas within massive elliptical galaxies; and the stellar metallicity gradients in low-surface brightness outskirts. We anticipate that the TNG50 dataset will have a long-lasting legacy value and constitute a platform for future programs which make detailed comparisons to astronomical observations as well as advance key aspects of galaxy formation theory. After a proprietary period of roughly one year, it will be made publicly available within the framework already developed for the first runs of the IllustrisTNG project [51].

4   Conclusions

Despite the tremendous theoretical and numerical achievements of recent large volume cosmological simulations such as Illustris, Eagle, or even TNG100 and TNG300, their limited mass and spatial resolution complicates the study of the structural details of galaxies less massive than a few times $10^9 \, M_\odot$. In contrast, projects focused on higher-resolution galaxy 'zoom' simulations have been less useful in broadly testing the outcome of their underlying physical models against population-wide morphological observed estimators because of their small sample sizes. For the most massive galaxy clusters, simulations with sufficient resolution to simultaneously model the co-evolving population of satellite galaxies have been prohibited by the large computational requirements as well as the complexity of the physical mechanisms which shape the circumgalactic and intracluster gas.

The TNG50 calculation that we have recently completed on the Hazel Hen machine is redefining the state-of-the-art of cosmological hydrodynamical simulations of galaxy formation by bridging the gap between large cosmological volumes and better resolved zoom galaxies. We have already showcased a few scientific applications of the TNG50 simulation and demonstrated that TNG50 is already proving to be an instrumental theoretical tool for the comparison—via mock observations of the simulated data—with existing and upcoming observational datasets. These include, for example, the abundances of dwarf galaxies in the first few billion years of the history of the Universe (with HST, JWST) and the kinematic properties of the Hα and molecular gas within and around galaxies at intermediate redshift (with e.g. integral field spectroscopy and other surveys, SINS/zC- SINF, PHIBBS, KMOS3D, ASPECS). Our analyses of TNG50 have also uncovered novel predictions, shedding new light on our understanding of galaxy evolution and providing a foundation for theoretical interpretation. Even beyond our currently-ongoing immediate scientific investigations, the TNG50 simulation will be a unique platform to pursue as of yet unimagined future projects, as we are now able to treat cosmological simulations as almost open ended laboratories for studying galaxy formation physics. The synthetic Universe of TNG50 will be a long term resource for the analysis, exploration and

interpretation of observations, one that we will make publicly available to the whole astronomy community.

References

1. M. Vogelsberger, S. Genel, V. Springel, P. Torrey, D. Sijacki, D. Xu, G. Snyder, D. Nelson, L. Hernquist, MNRAS **444**, 1518 (2014). https://doi.org/10.1093/mnras/stu1536
2. M. Vogelsberger, S. Genel, V. Springel, P. Torrey, D. Sijacki, D. Xu, G. Snyder, S. Bird, D. Nelson, L. Hernquist, Nature **509**, 177 (2014). https://doi.org/10.1038/nature13316
3. S. Genel, M. Vogelsberger, V. Springel, D. Sijacki, D. Nelson, G. Snyder, V. Rodriguez-Gomez, P. Torrey, L. Hernquist, MNRAS **445**, 175 (2014). https://doi.org/10.1093/mnras/stu1654
4. D. Sijacki, M. Vogelsberger, S. Genel, V. Springel, P. Torrey, G.F. Snyder, D. Nelson, L. Hernquist, MNRAS **452**, 575 (2015). https://doi.org/10.1093/mnras/stv1340
5. J. Schaye, R.A. Crain, R.G. Bower, M. Furlong, M. Schaller, T. Theuns, C. Dalla Vecchia, C.S. Frenk, I.G. McCarthy, J.C. Helly, A. Jenkins, Y.M. Rosas-Guevara, S.D.M. White, M. Baes, C.M. Booth, P. Camps, J.F. Navarro, Y. Qu, A. Rahmati, T. Sawala, P.A. Thomas, J. Trayford, MNRAS **446**, 521 (2015). https://doi.org/10.1093/mnras/stu2058
6. R.A. Crain, J. Schaye, R.G. Bower, M. Furlong, M. Schaller, T. Theuns, C. Dalla Vecchia, C.S. Frenk, I.G. McCarthy, J.C. Helly, A. Jenkins, Y.M. Rosas-Guevara, S.D.M. White, J.W. Trayford, MNRAS **450**, 1937 (2015). https://doi.org/10.1093/mnras/stv725
7. Y. Dubois, S. Peirani, C. Pichon, J. Devriendt, R. Gavazzi, C. Welker, M. Volonteri, MNRAS **463**, 3948 (2016). https://doi.org/10.1093/mnras/stw2265
8. A. Pillepich, V. Springel, D. Nelson, S. Genel, J. Naiman, R. Pakmor, L. Hernquist, P. Torrey, M. Vogelsberger, R. Weinberger, F. Marinacci, MNRAS **473**, 4077 (2018). https://doi.org/10.1093/mnras/stx2656
9. R. Weinberger, V. Springel, L. Hernquist, A. Pillepich, F. Marinacci, R. Pakmor, D. Nelson, S. Genel, M. Vogelsberger, J. Naiman, P. Torrey, MNRAS **465**, 3291 (2017). https://doi.org/10.1093/mnras/stw2944
10. A. Pillepich, D. Nelson, L. Hernquist, V. Springel, R. Pakmor, P. Torrey, R. Weinberger, S. Genel, J.P. Naiman, F. Marinacci, M. Vogelsberger, MNRAS **475**, 648 (2018). https://doi.org/10.1093/mnras/stx3112
11. V. Springel, R. Pakmor, A. Pillepich, R. Weinberger, D. Nelson, L. Hernquist, M. Vogelsberger, S. Genel, P. Torrey, F. Marinacci, J. Naiman, MNRAS **475**, 676 (2018). https://doi.org/10.1093/mnras/stx3304
12. D. Nelson, A. Pillepich, V. Springel, R. Weinberger, L. Hernquist, R. Pakmor, S. Genel, P. Torrey, M. Vogelsberger, G. Kauffmann, F. Marinacci, J. Naiman, MNRAS **475**, 624 (2018). https://doi.org/10.1093/mnras/stx3040
13. F. Marinacci, M. Vogelsberger, R. Pakmor, P. Torrey, V. Springel, L. Hernquist, D. Nelson, R. Weinberger, A. Pillepich, J. Naiman, S. Genel, ArXiv e-prints (2017)
14. J.P. Naiman, A. Pillepich, V. Springel, E. Ramirez-Ruiz, P. Torrey, M. Vogelsberger, R. Pakmor, D. Nelson, F. Marinacci, L. Hernquist, R. Weinberger, S. Genel, ArXiv e-prints (2017)
15. D. Nelson, A. Pillepich, S. Genel, M. Vogelsberger, V. Springel, P. Torrey, V. Rodriguez-Gomez, D. Sijacki, G.F. Snyder, B. Griffen, F. Marinacci, L. Blecha, L. Sales, D. Xu, L. Hernquist, Astronomy Comput. **13**, 12 (2015). https://doi.org/10.1016/j.ascom.2015.09.003

16. V. Springel, MNRAS **401**, 791 (2010). https://doi.org/10.1111/j.1365-2966.2009.15715.x
17. R. Pakmor, A. Bauer, V. Springel, MNRAS **418**, 1392 (2011). https://doi.org/10.1111/j.1365-2966.2011.19591.x
18. R. Pakmor, V. Springel, MNRAS **432**, 176 (2013). https://doi.org/10.1093/mnras/stt428
19. R. Pakmor, V. Springel, A. Bauer, P. Mocz, D.J. Munoz, S.T. Ohlmann, K. Schaal, C. Zhu, MNRAS **455**, 1134 (2016). https://doi.org/10.1093/mnras/stv2380
20. D. Nelson, A. Pillepich, V. Springel, R. Weinberger, L. Hernquist, R. Pakmor, S. Genel, P. Torrey, M. Vogelsberger, G. Kauffmann, F. Marinacci, J. Naiman,
21. V. Springel, L. Hernquist, MNRAS **339**, 289 (2003). https://doi.org/10.1046/j.1365-8711.2003.06206.x
22. S. Genel, D. Nelson, A. Pillepich, V. Springel, R. Pakmor, R. Weinberger, L. Hernquist, J. Naiman, M. Vogelsberger, F. Marinacci, P. Torrey, MNRAS **474**, 3976 (2018). https://doi.org/10.1093/mnras/stx3078
23. J.P. Naiman, A. Pillepich, V. Springel, E. Ramirez-Ruiz, P. Torrey, M. Vogelsberger, R. Pakmor, D. Nelson, F. Marinacci, L. Hernquist, R. Weinberger, S. Genel, MNRAS **477**, 1206 (2018). https://doi.org/10.1093/mnras/sty618
24. R. Weinberger, V. Springel, R. Pakmor, D. Nelson, S. Genel, A. Pillepich, M. Vogelsberger, F. Marinacci, J. Naiman, P. Torrey, L. Hernquist, ArXiv e-prints (2018)
25. M. Habouzit, S. Genel, R.S. Somerville, D. Kocevski, M. Hirschmann, A. Dekel, E. Choi, D. Nelson, A. Pillepich, P. Torrey, L. Hernquist, M. Vogelsberger, R. Weinberger, V. Springel, ArXiv e-prints (2018)
26. P. Torrey, M. Vogelsberger, F. Marinacci, R. Pakmor, V. Springel, D. Nelson, J. Naiman, A. Pillepich, S. Genel, R. Weinberger, L. Hernquist, ArXiv e-prints (2017)
27. M.R. Lovell, A. Pillepich, S. Genel, D. Nelson, V. Springel, R. Pakmor, F. Marinacci, R. Weinberger, P. Torrey, M. Vogelsberger, L. Hernquist, ArXiv e-prints (2018)
28. V. Rodriguez-Gomez, G.F. Snyder, J.M. Lotz, D. Nelson, A. Pillepich, V. Springel, S. Genel, R. Weinberger, S. Tacchella, R. Pakmor, P. Torrey, F. Marinacci, M. Vogelsberger, L. Hernquist, D.A. Thilker, MNRAS **483**, 4140 (2019). https://doi.org/10.1093/mnras/sty3345
29. Q. Zhu, D. Xu, M. Gaspari, V. Rodriguez-Gomez, D. Nelson, M. Vogelsberger, P. Torrey, A. Pillepich, J. Zjupa, R. Weinberger, F. Marinacci, R. Pakmor, S. Genel, Y. Li, V. Springel, L. Hernquist, MNRAS **480**, L18 (2018). https://doi.org/10.1093/mnrasl/sly111
30. K. Yun, A. Pillepich, E. Zinger, D. Nelson, M. Donnari, G. Joshi, V. Rodriguez-Gomez, S. Genel, R. Weinberger, M. Vogelsberger, L. Hernquist, MNRAS (2018). https://doi.org/10.1093/mnras/sty3156
31. M. Vogelsberger, F. Marinacci, P. Torrey, S. Genel, V. Springel, R. Weinberger, R. Pakmor, L. Hernquist, J. Naiman, A. Pillepich, D. Nelson, MNRAS **474**, 2073 (2018). https://doi.org/10.1093/mnras/stx2955
32. D.J. Barnes, M. Vogelsberger, R. Kannan, F. Marinacci, R. Weinberger, V. Springel, P. Torrey, A. Pillepich, D. Nelson, R. Pakmor, J. Naiman, L. Hernquist, M. McDonald, MNRAS **481**, 1809 (2018). https://doi.org/10.1093/mnras/sty2078
33. D. Nelson, G. Kauffmann, A. Pillepich, S. Genel, V. Springel, R. Pakmor, L. Hernquist, R. Weinberger, P. Torrey, M. Vogelsberger, F. Marinacci, MNRAS (2018). https://doi.org/10.1093/mnras/sty656
34. A. Gupta, T. Yuan, P. Torrey, M. Vogelsberger, D. Martizzi, K.V.H. Tran, L.J. Kewley, F. Marinacci, D. Nelson, A. Pillepich, L. Hernquist, S. Genel, V. Springel, MNRAS **477**, L35 (2018). https://doi.org/10.1093/mnrasl/sly037
35. Y. Wang, M. Vogelsberger, D. Xu, S. Mao, V. Springel, H. Li, D. Barnes, L. Hernquist, A. Pillepich, F. Marinacci, R. Pakmor, R. Weinberger, P. Torrey, ArXiv e-prints (2018)
36. D. Martizzi, M. Vogelsberger, M.C. Artale, M. Haider, P. Torrey, F. Marinacci, D. Nelson, A. Pillepich, R. Weinberger, L. Hernquist, J. Naiman, V. Springel, ArXiv e-prints (2018)
37. F. Villaescusa-Navarro, S. Genel, E. Castorina, A. Obuljen, D.N. Spergel, L. Hernquist, D. Nelson, I.P. Carucci, A. Pillepich, F. Marinacci, B. Diemer, M. Vogelsberger, R. Weinberger, R. Pakmor, ApJ **866**, 135 (2018). https://doi.org/10.3847/1538-4357/aadba0

38. B. Diemer, A.R.H. Stevens, J.C. Forbes, F. Marinacci, L. Hernquist, C.d.P. Lagos, A. Sternberg, A. Pillepich, D. Nelson, G. Popping, F. Villaescusa-Navarro, P. Torrey, M. Vogelsberger, ApJS **238**, 33 (2018). https://doi.org/10.3847/1538-4365/aae387

39. A.R.H. Stevens, B. Diemer, C.d.P. Lagos, D. Nelson, A. Pillepich, T. Brown, B. Catinella, L. Hernquist, R. Weinberger, M. Vogelsberger, F. Marinacci, ArXiv e-prints (2018)

40. G. Popping, A. Pillepich, R.S. Somerville, R. Decarli, F. Walter, M. Aravena, C. Carilli, P. Cox, D. Nelson, D. Riechers, A. Weiss, L. Boogaard, R. Bouwens, T. Contini, P.C. Cortes, E. da Cunha, E. Daddi, T. Díaz-Santos, B. Diemer, J. González-López, L. Hernquist, R. Ivison, O. Le Fevre, F. Marinacci, H.W. Rix, M. Swinbank, M. Vogelsberger, P. van der Werf, J. Wagg, L.Y.A. Yung, arXiv e-prints (2019)

41. M. Ntampaka, J. ZuHone, D. Eisenstein, D. Nagai, A. Vikhlinin, L. Hernquist, F. Marinacci, D. Nelson, R. Pakmor, A. Pillepich, P. Torrey, M. Vogelsberger, ArXiv e-prints (2018)

42. M. Huertas-Company, V. Rodriguez-Gomez, D. Nelson, A. Pillepich, M. Bernardi, H. Domínguez-Sánchez, S. Genel, R. Pakmor, G.F. Snyder, M. Vogelsberger, arXiv e-prints (2019)

43. R.J.J. Grand, F.A. Gómez, F. Marinacci, R. Pakmor, V. Springel, D.J.R. Campbell, C.S. Frenk, A. Jenkins, S.D.M. White, ArXiv e-prints (2016)

44. P.F. Hopkins, A. Wetzel, D. Keres, C.A. Faucher-Giguere, E. Quataert, M. Boylan-Kolchin, N. Murray, C.C. Hayward, S. Garrison-Kimmel, C. Hummels, R. Feldmann, P. Torrey, X. Ma, D. Angles-Alcazar, K.Y. Su, M. Orr, D. Schmitz, I. Escala, R. Sanderson, M.Y. Grudic, Z. Hafen, J.H. Kim, A. Fitts, J.S. Bullock, C. Wheeler, T.K. Chan, O.D. Elbert, D. Narananan, ArXiv e-prints (2017)

45. A. Pillepich, D. Nelson, V. Springel, R. Pakmor, P. Torrey, R. Weinberger, M. Vogelsberger, F. Marinacci, S. Genel, A. van der Wel, L. Hernquist, arXiv e-prints arXiv:1902.05553 (2019)

46. D. Nelson, A. Pillepich, V. Springel, R. Pakmor, R. Weinberger, S. Genel, P. Torrey, M. Vogelsberger, F. Marinacci, L. Hernquist, arXiv e-prints arXiv:1902.05554 (2019)

47. M. Vogelsberger, D. Nelson, A. Pillepich, X. Shen, F. Marinacci, V. Springel, R. Pakmor, S. Tacchella, R. Weinberger, P. Torrey, L. Hernquist, arXiv e-prints arXiv:1904.07238 (2019)

48. N.M. Förster Schreiber, A. Renzini, C. Mancini, R. Genzel, N. Bouché, G. Cresci, E.K.S. Hicks, S.J. Lilly, Y. Peng, A. Burkert, C.M. Carollo, A. Cimatti, E. Daddi, R.I. Davies, S. Genel, J.D. Kurk, P. Lang, D. Lutz, V. Mainieri, H.J. McCracken, M. Mignoli, T. Naab, P. Oesch, L. Pozzetti, M. Scodeggio, K. Shapiro Griffin, A.E. Shapley, A. Sternberg, S. Tacchella, L.J. Tacconi, S. Wuyts, G. Zamorani, ArXiv e-prints (2018)

49. H.R. Russell, J.S. Sanders, A.C. Fabian, S.A. Baum, M. Donahue, A.C. Edge, B.R. McNamara, C.P. O'Dea, MNRAS **406**, 1721 (2010). https://doi.org/10.1111/j.1365-2966.2010.16822.x

50. H.J. Mo, S. Mao, S.D.M. White, MNRAS **295**, 319 (1998). https://doi.org/10.1046/j.1365-8711.1998.01227.x

51. D. Nelson, V. Springel, A. Pillepich, V. Rodriguez-Gomez, P. Torrey, S. Genel, M. Vogelsberger, R. Pakmor, F. Marinacci, R. Weinberger, L. Kelley, M. Lovell, B. Diemer, L. Hernquist, arXiv e-prints arXiv:1812.05609 (2018)